SMALL DEBRIS IMPACT SIMULATION USING MSC/DYTRAN

Franco Olmi
Kennedy Diniz do Nascimento
EMBRAER - Empresa Brasileira de Aeronáutica,
Structural Analysis Department
12227-901, São José dos Campos- SP - **Brazil**
E-mail: estemb@embraer.com.br

ABSTRACT

The problem of rotor blade fragment impact against an airplane structure (representing the "Small Debris" effect, due to rotor burst) has been investigated. The simulations were performed using the MSC/DYTRAN software, taking into account some different approaches, such as the influence of the finite elements modeling as well as the material behavior (involving characteristics like constitutive law, strain rate effects and failure modes). Finally, to corroborate the analysis, the numerical results were compared with experimental data.

1.0 INTRODUCTION

Rotor engine failures can result in high velocity fragment impacts in aircraft adjacent structures. This can result in serious damage to important components, such fuel tank, hydraulic systems and surface controls. Specifically in the case of the rotor burst, some small fragments (also called small debris) cannot be contained by the engine housing and in this situation, the hazard must be taken into account by means of design procedures.
This paper is related with the small debris analysis based on a numerical approach, using the MSC/DYTRAN code, simulating the impact of small debris against a typical aircraft fuselage region. In order to corroborate the analysis, experimental data were compared with the numerical analysis.

2.0 ANALYSIS

2.1 FINITE ELEMENT MODELING

The model herein analyzed represents a typical aircraft fuselage region, whose principal components are:

- skin;
- stringers;
- frames.

The skin was modeled as a plane plate using 40880 quadrilateral shell elements (**CQUAD4**, **KEYHOFF** formulation, with 5 integration points).
The skin material (Aluminum 2024) behavior was modeled using the Johnson & Cook yield model:

$$s_y = (A + B \cdot e_p^n) \cdot [1 - C \cdot \ln(\frac{\dot{e}}{\dot{e}_0})] \cdot [1 - \left(\frac{T - T_r}{T_m - T_r} \right)^k] \qquad (2.1\text{-}1)$$

where the constants are:

A = static yield stress = 265 MPa
B = hardening modulus = 426 MPa
n = hardening exponent = 0.34
C = strain rate parameter = 0.015
$\dot{\varepsilon}_0$ = reference strain rate = 1 s^{-1}
T_r = room temperature = 293 K
T_m = melt temperature = 775 K
k = temperature exponent = 1

The above values were obtained from the MSC/MVISION database. The **FAILMPS** entry was used to represent the element failure model. Although the MSC/MVISION database presents a value of 0.5 for this entry, a value of 0.18 was used, whose seems more realistic, according to the test results.
Frames and stringers were modeled by bar elements (**CBEAM**), using the Von Mises yield criteria to represent the material behavior.
The rotor fragment (small debris, that impacts against the skin) was considered as rigid body, modeled using the rigid elipsoid element (representing a sphere of 22mm diameter and mass of 43.45g) with nodal initial velocity as the loading condition. The skin border was constrained as a simply supported plate (see figure 2.2-1). MSC/DYTRAN Lagrangian formulation was used to perform the simulation. No friction effects were considered. Adaptive contact between the rigid elipsoid and Lagrangian grid points was defined by the **CONTREL** card. The simulated impact positions were defined according to the results obtained in the experiments:

Plate thickness (mm)	Nominal energy (J)	"x" position	"y" position
1.6	250	-10	25
1.6	500	0	-46
1.6	750	10	30
3.2	500	15	-22
3.2	1000	28	33
3.2	1500	24	-36

Table 2.1-1 - Simulated impact positions.

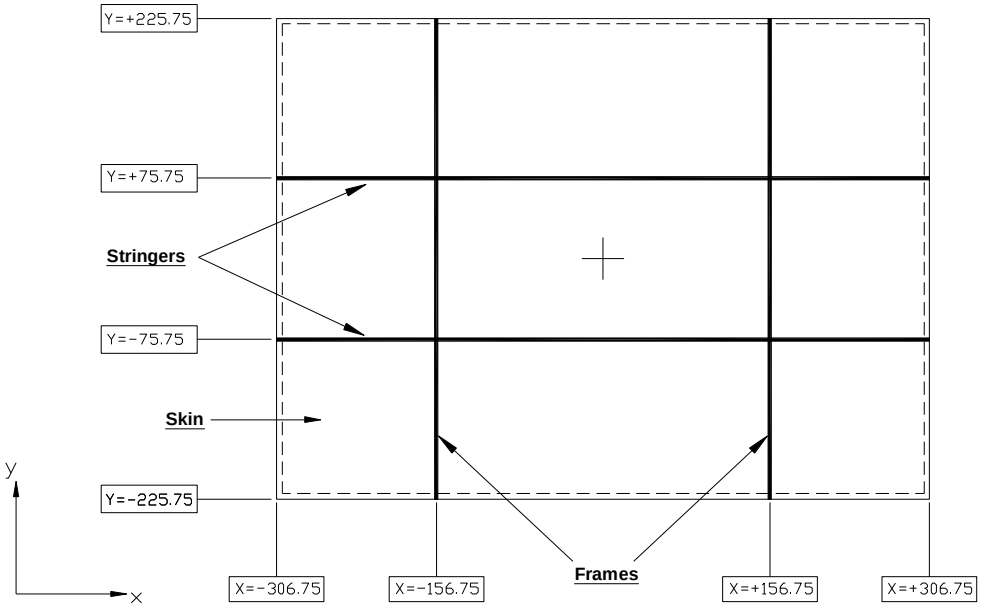

Figure 2.1-1 - Schematic representation of the model.

2.2 EXPERIMENTAL PROCEDURES

To corroborate the numerical analysis, several tests were performed. In the first test set, three 1.6 thick aluminum plates were evaluated, with energy levels of 250J, 500J and 750J. The second set was composed of three 3.2 thick aluminum plate, with energy levels of 500J, 1000J and 1500J.
The test specimens are represented in Fig. 2.2-1, whose dimensions are the same as those used in the numerical analysis.

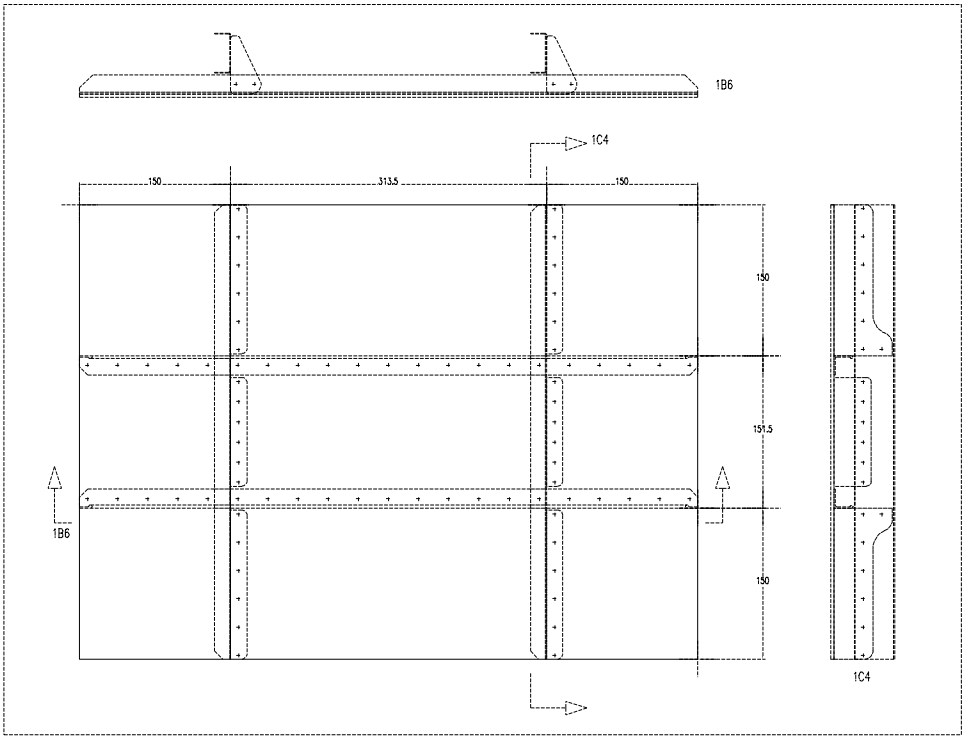

Figure 2.2-1 - Test specimen.

Two high speed cameras were used to record the initial (V_i - before the impact) and final (V_f - after the impact) velocities. The main components of test set-up (see figure 2.2-2) are the following:

- cannon: to provide the initial velocity of the sphere (v_0);
- barrier: to retain the sphere after the impact (when the perforation of the plate occurs);
- cameras: two high speed cameras (cam 1 & cam 2), to record the initial (v_0) and final (v_f) sphere velocities, respectively.

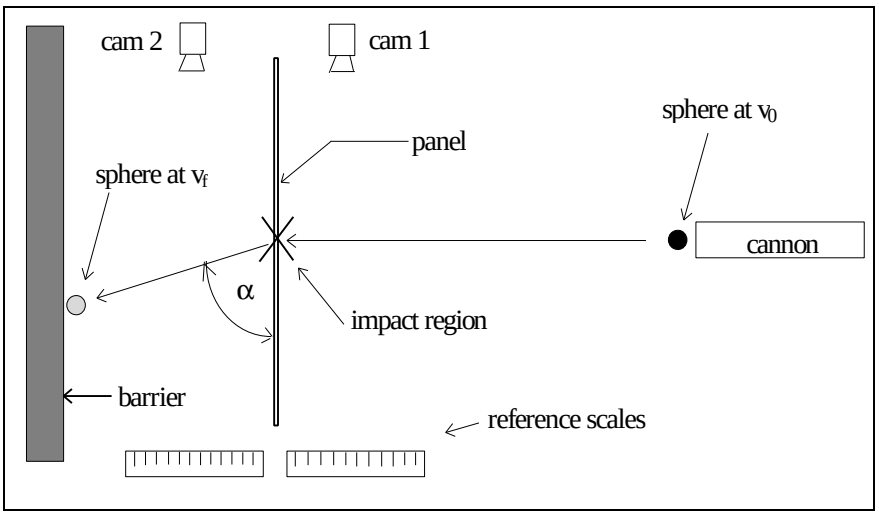

Figure 2.2-2 - Test assembly.

2.3 COMPARISON BETWEEEN NUMERICAL AND EXPERIMENTAL RESULTS

The following graphics and tables shows a comparison between numerical and experimental results.

		Experimental	**Numerical**
Plate thickness (mm)	*Initial sphere speed (m/s)*	*Final measured sphere speed (m/s)*	*Final Dytran sphere speed (m/s)*
1.6	113.8	52.3	96.9
1.6	153.4	129.7	140.9
1.6	183.8	174.2	173.0
3.2	155.8	114.0	116.0
3.2	205.8	188.8	175.8
3.2	257.9	254.6	232.9

Table 2.3-1 - Final sphere speed comparison (experimental vs numerical)

		Experimental	**Numerical**
Plate thickness (mm)	*Initial sphere energy (J)*	*Final sphere energy (J)*	*Final sphere energy (J)*
1.6	281.6	59.4	204.2
1.6	511.3	365.3	431.4
1.6	734.0	659.0	650.4
3.2	527.4	282.3	292.6
3.2	920.0	774.1	671.2
3.2	1445.4	1408.8	1178.9

Table 2.3-2 - Final sphere energy comparison (experimental vs numerical)

		Experimental	Numerical
Plate thickness (mm)	*Initial sphere energy (J)*	*(Initial - Final) energy DE (J)*	*(Initial - Final) energy Delta E (J)*
1.6	281.6	222.1	77.4
1.6	511.3	146.0	79.9
1.6	734.0	75.0	83.6
3.2	527.4	245.1	234.8
3.2	920.0	146.0	248.9
3.2	1445.4	36.6	266.5

Table 2.3-3 - Energy variation comparison (experimental vs numerical)

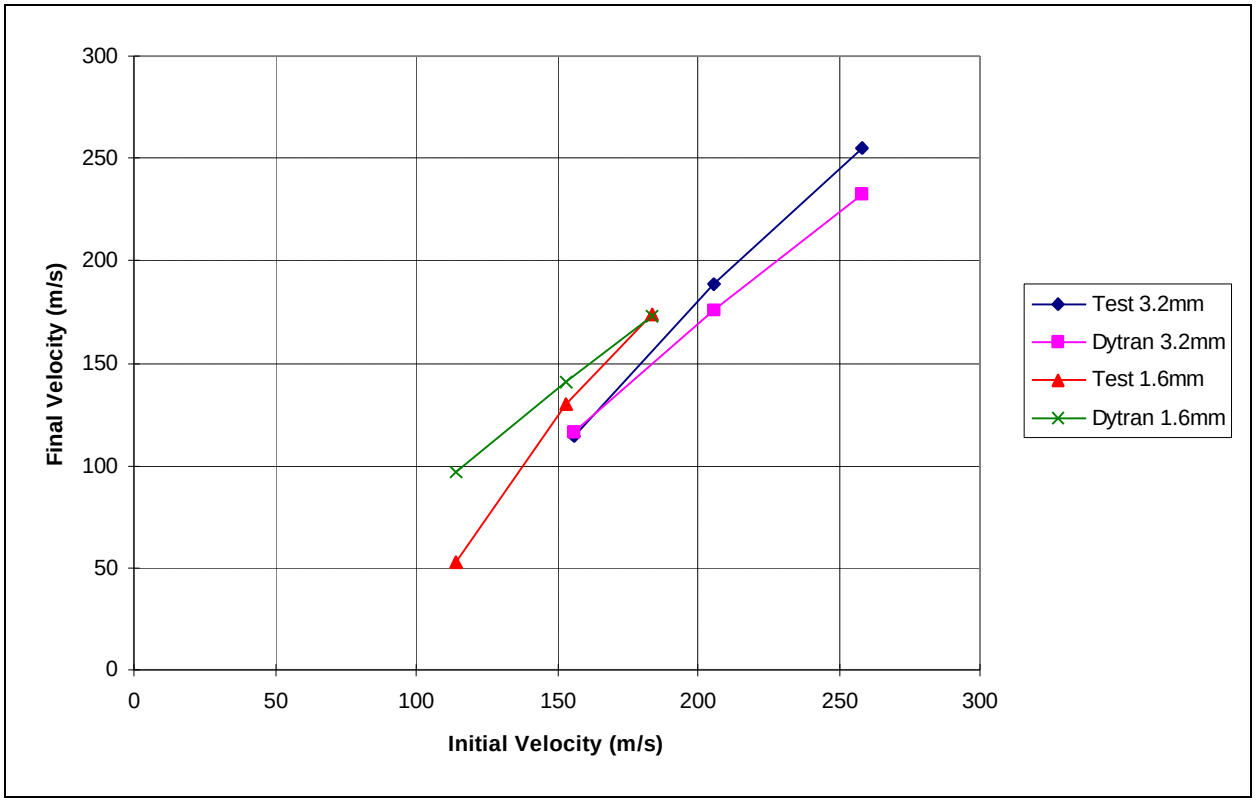

Figure 2.3-1 - Comparison between initial and final sphere velocity.

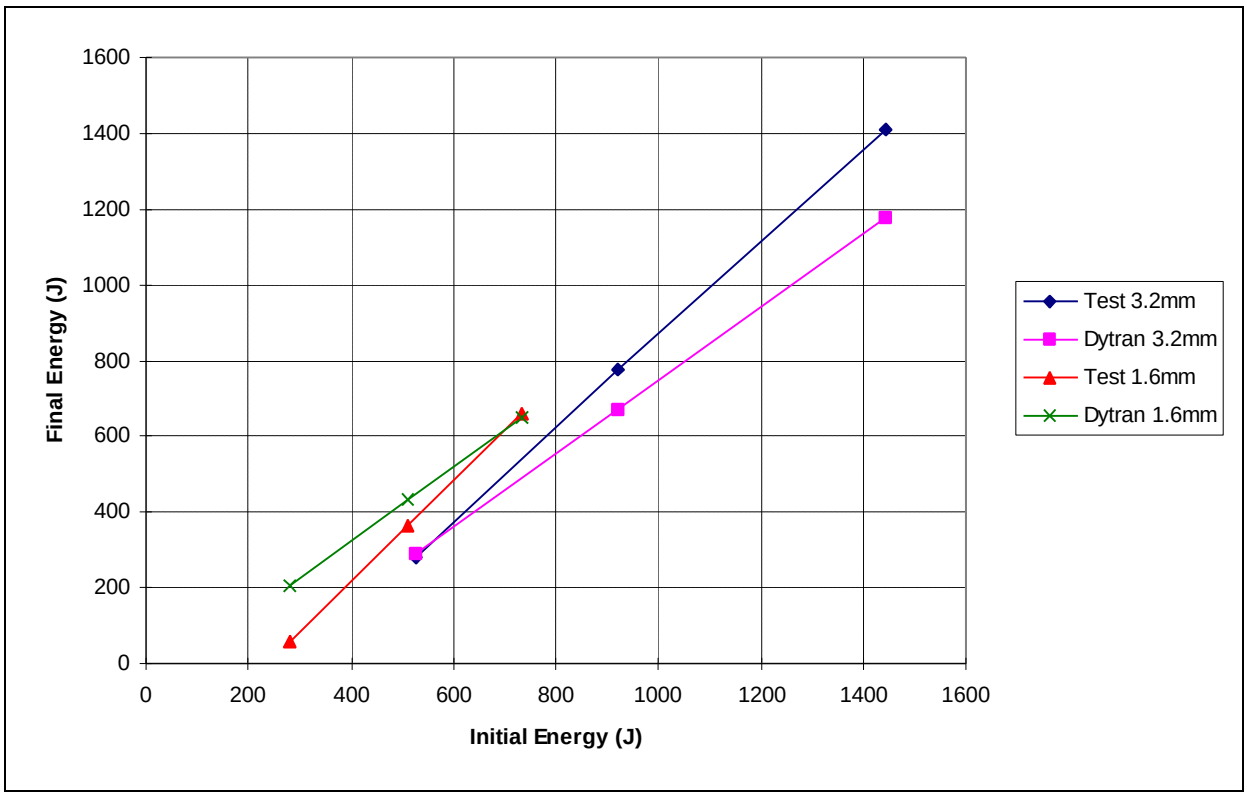

Figure 2.3-2 - Comparison between initial and final sphere energy.

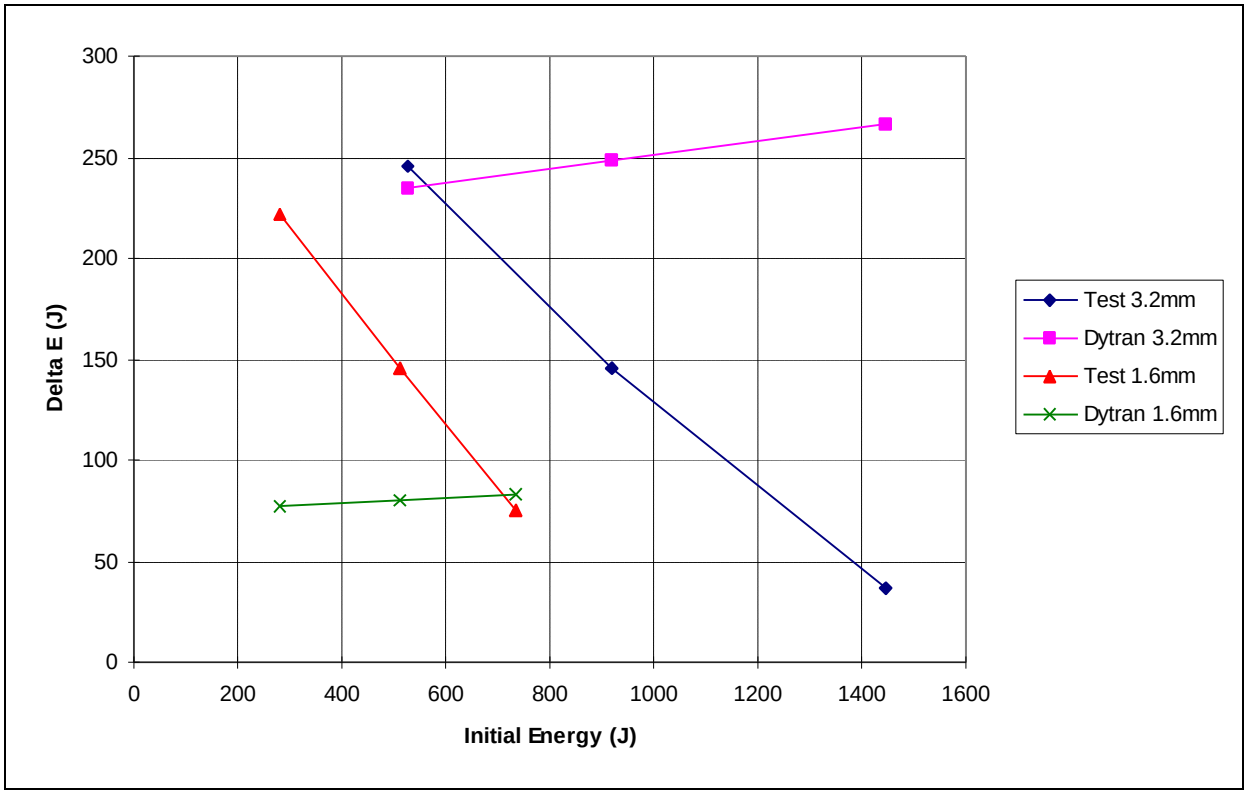

Figure 2.3-3 - Comparison between initial energy and energy variation.

3.0 DISCUSSION

Several FE models of the skin were tested, including models with lagrangian shell (**CQUAD4**) or lagrangian solid elements (**CHEXA**). Based on experimental data, shell elements presents the best results when compared with solids elements.
The sphere was modeled in three different ways: as a rigid body (**RELLIPS**, rigid elipsoid), by rigid plate elements (**MATRIG**) and by lagrangian solid elements (**CHEXA**). No important differences were observed between these three models. For this reason, the rigid elipsoid was chosen, due its modeling facility and lower computational cost. Stringers and frames also were modeled by different element types (shells and bars). For the same reason explained previously, we prefer to use bar elements.
The material behavior was simulated by two models: the first one (Johnson & Cook - **YLDJC**), where the yield stress is a function of the effective plastic strain, strain rate and temperature and the other, (Von Mises - **YLDVM**), considering a piecewise-linear yield model, with isotropic hardening. In all simulations both models presented very similar results. However, the Johnson & Cook model was chosen, specially due to its more accurate modeling of the strain rate parameter.
Some discrepancies between numerical and experimental results were observed. The most important aspect is the opposite behavior presented by the simulation, when compared with the experiments. The experiments shown an upward slope in figure 2.3-3, indicating that the plates retain less energy at higher impact velocities. The simulation results shown a downward slope, indicating that the plates retain more energy at higher impact velocities. Both thin and thick plates presents the same behavior.

4.0 CONCLUSIONS

The finite element model used can be considered adequate for this kind of simulation. Also, the constitutive material law (Johnson & Cook) seems to be the most correct , as it consider strain rate and thermal effects in its model. A comparison between experimental and numerical deformed shapes after the impact are showed in section **FIGURES**.
Although some MSC/DYTRAN results shown good agreement with the experiments, some aspects needs to be evaluated more accurately and some refinements related with the material behavior model needs to be made. In particular, we can suppose that the effect of the strain rate parameter plays an important role in the results, specially when modeling high velocity impacts. In such cases, very high strain rates may be occur, with the flow stress being highly rate-sensitive. In the same way, the failure parameter (**FAILMPS**, considered constant in all simulations) have a direct relationship with the strain rate, what could explain the differences between simulations and tests. At this time we (in conjunction with the MSC/DYTRAN technical support team) remains investigating the problem, in order to improve the current results.
Finally, is spite of the discrepancies previously mentioned, we can conclude that MSC/DYTRAN is a powerful tool to simulate small debris impacts in typical aircraft fuselage panels.

5.0 ACKNOWLEDGEMENTS

The authors would like to thank the personnel at EMBRAER **EST** and **NST** departments, for their support of this work.

6.0 REFERENCES

(1) MSC/DYTRAN *User's Manual Version 4.0*, The MacNeal-Schwendler Corporation, Los Angeles, CA, November 1997.

(2) MSC/DYTRAN *Example Problem Manual Version 3.0*, The MacNeal-Schwendler Corporation, Los Angeles, CA, February 1996.

(3) Chen, E. P., "Finite element simulation of perforation and penetration of aluminum targets by conical-nosed rods", *Mechanics of Materials* 10, 1990, pp. 107-115.

(4) Camacho, G. T. and Ortiz, M., "Adaptive Lagrangian modeling of ballistic penetration of metallic targets", *Comput. Methods Appl. Mech. Engrg*. 142, 1997, pp. 269-301.

(5) Kelvin Y. Ng., "Turbine Rotor Burst Containment Analysis Using MSC/DYTRAN", MSC 1996 World User's Conference Proceedings, Newport Beach, 1996.

FIGURES

The following figures shown a comparison between experimental and numerical deformed shapes after the impacts.

Experimental result (Nominal energy: 250J, plate thickness 1.6mm)

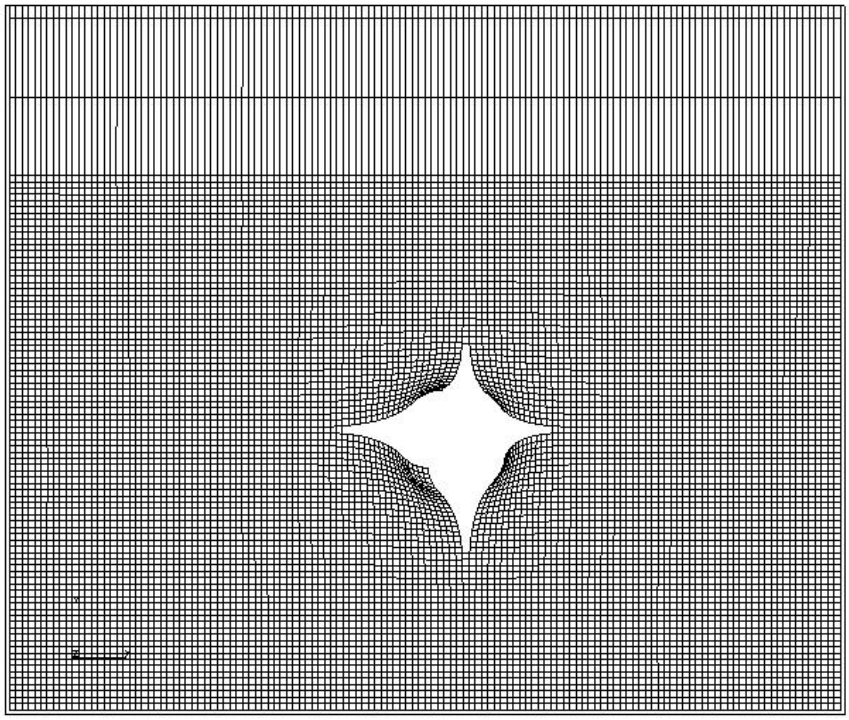

Dytran result (Nominal energy: 250J, plate thickness 1.6mm)

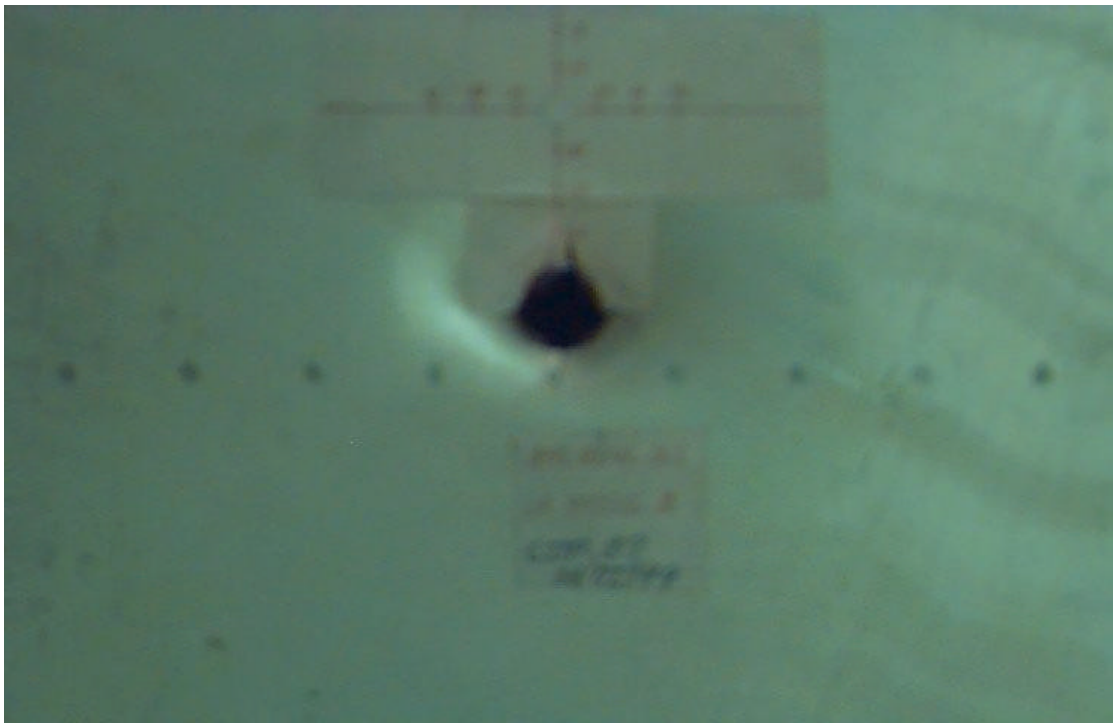

Experimental result (Nominal energy: 500J, plate thickness 1.6mm)

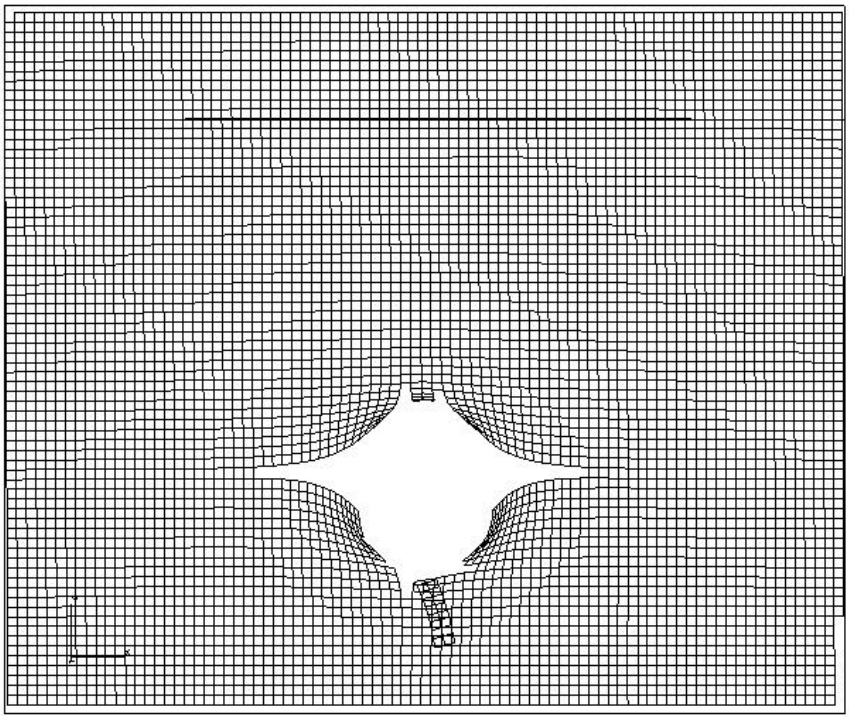

Dytran result (Nominal energy: 500J, plate thickness 1.6mm)

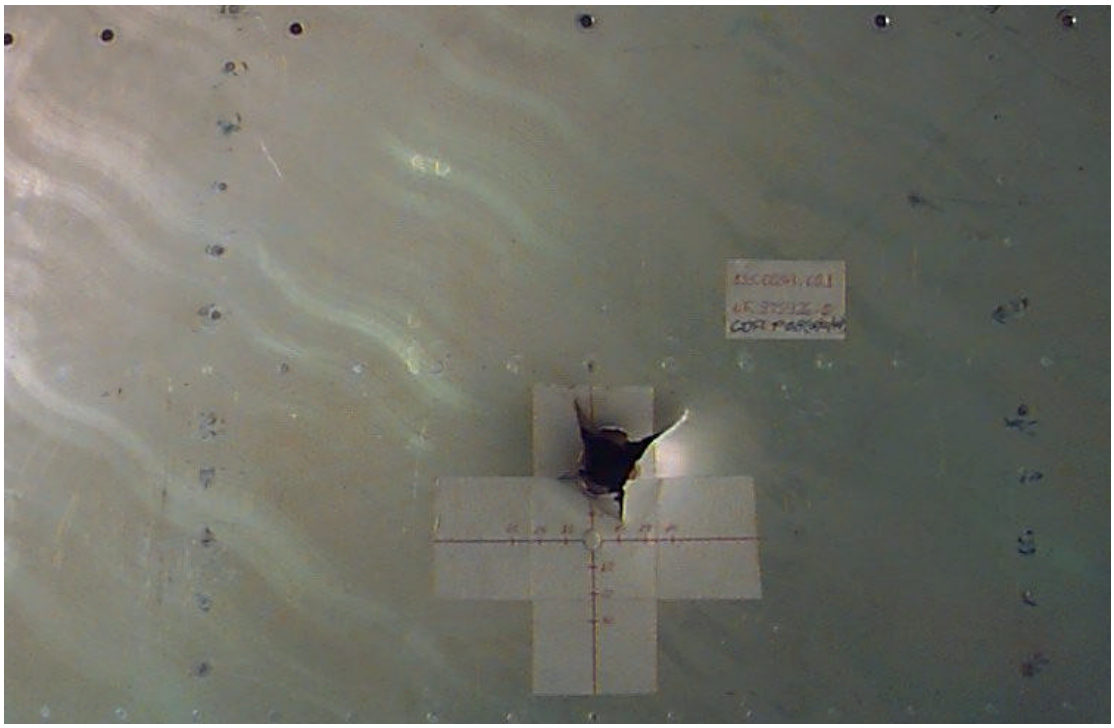

Experimental result (Nominal energy: 750J, plate thickness 1.6mm)

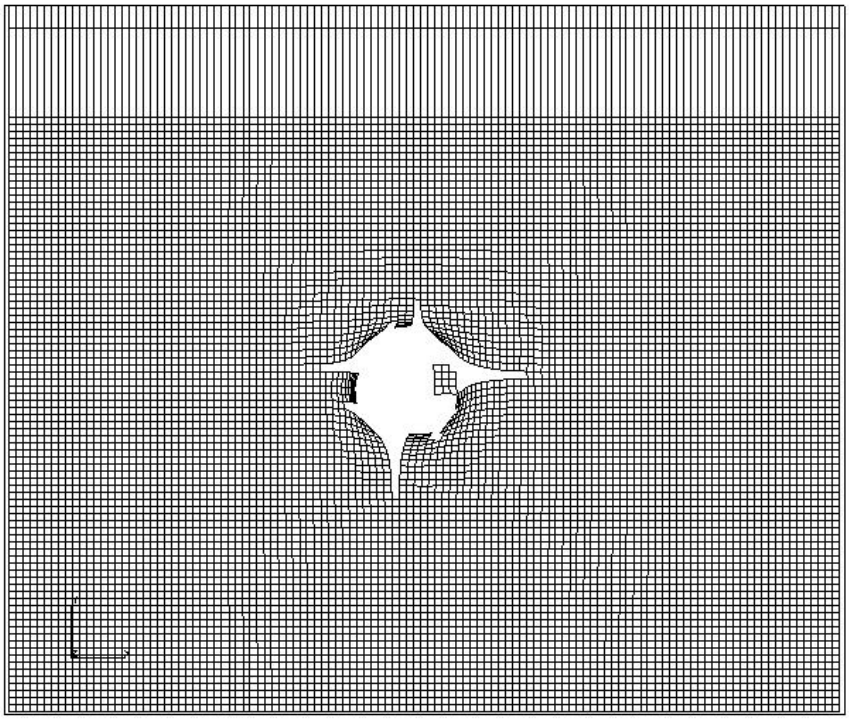

Dytran result (Nominal energy: 750J, plate thickness 1.6mm)

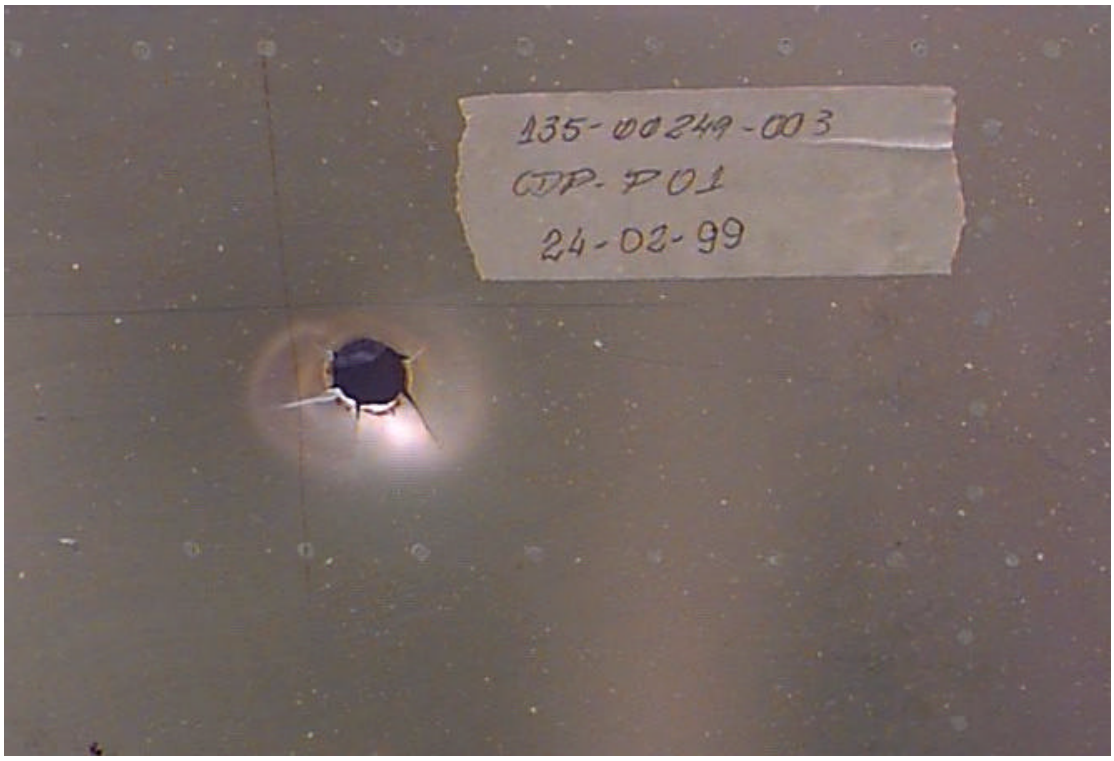

Experimental result (Nominal energy: 500J, plate thickness 3.2 mm)

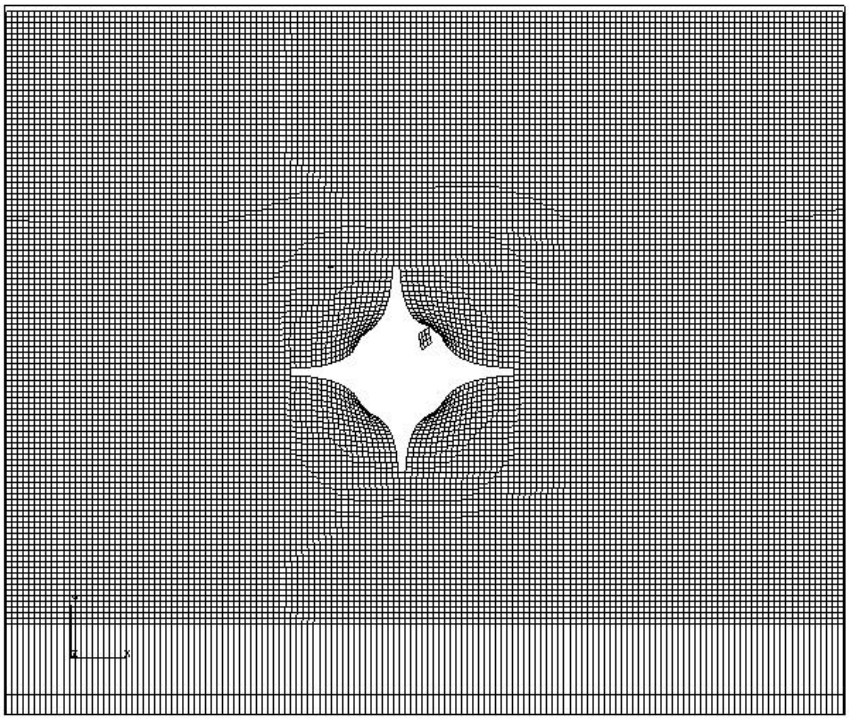

Dytran result (Nominal energy: 500J, plate thickness 3.2 mm)

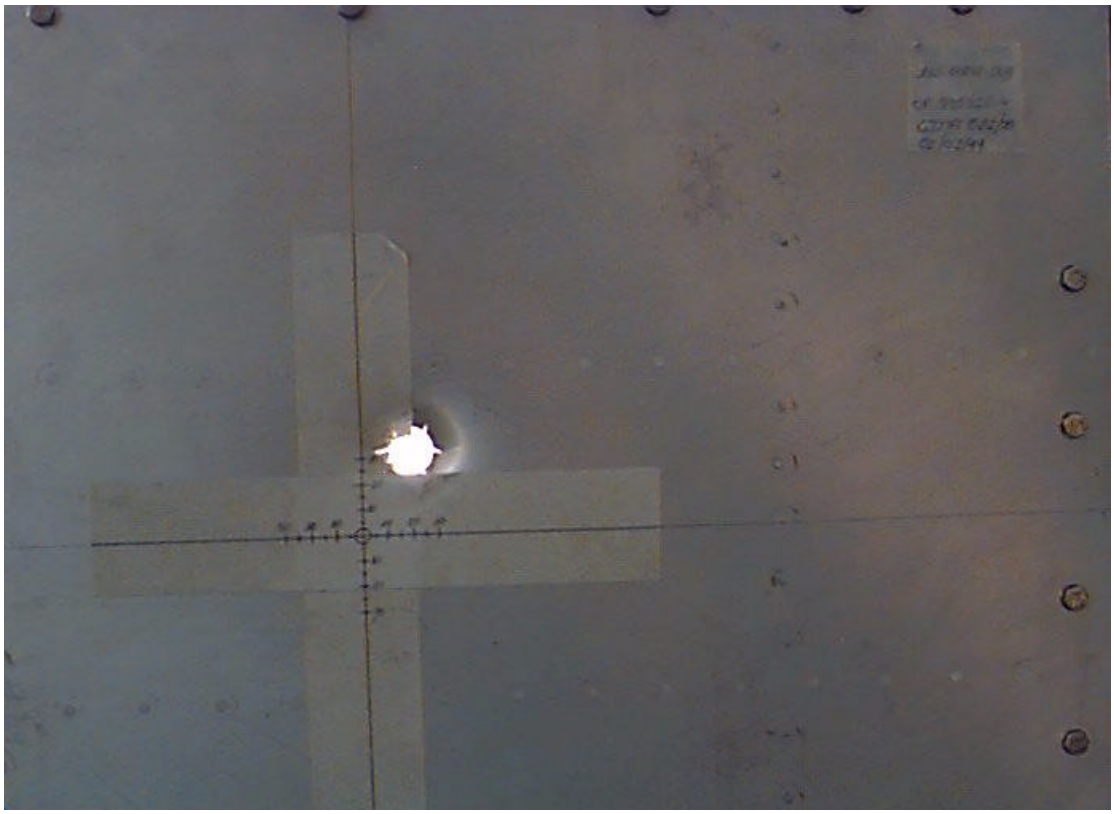

Experimental result (Nominal energy: 1000J, plate thickness 3.2 mm)

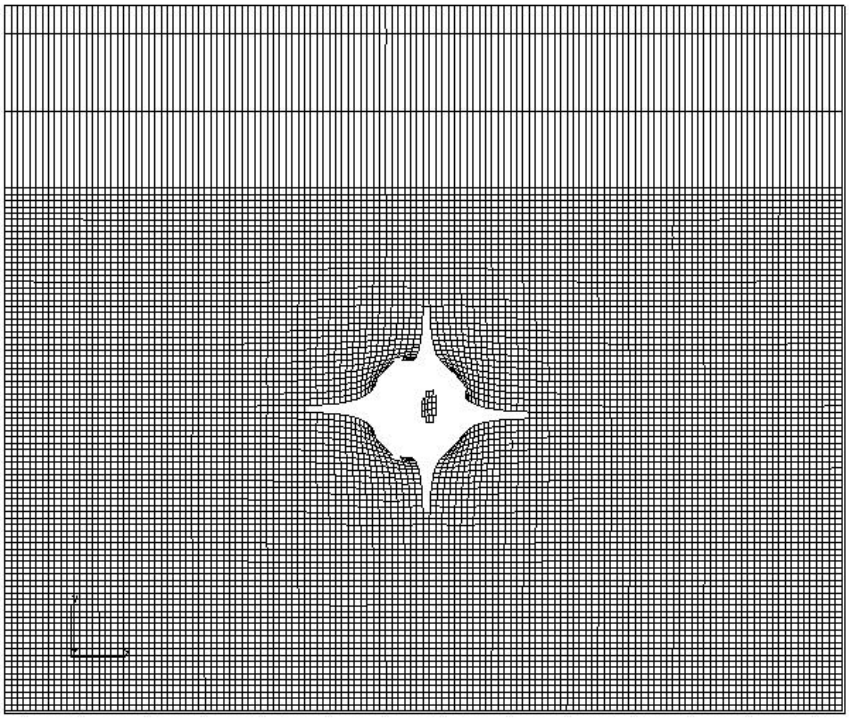

Dytran result (Nominal energy: 1000J, plate thickness 3.2 mm)

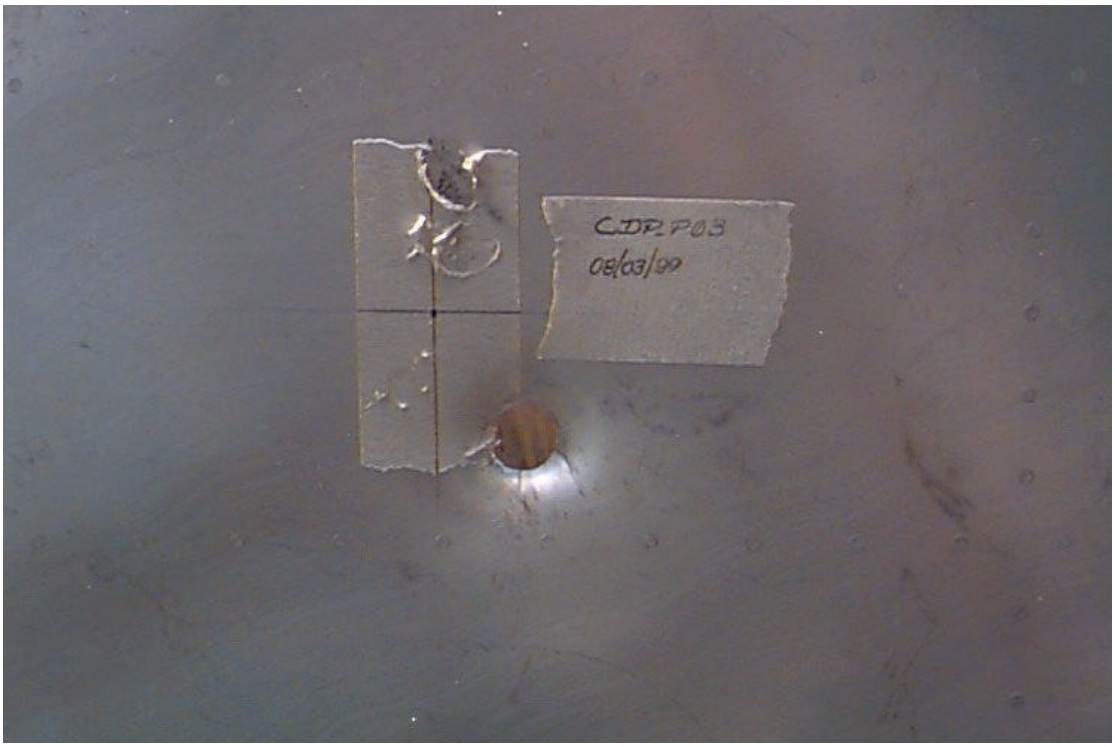

Experimental result (Nominal energy: 1500J, plate thickness 3.2 mm)

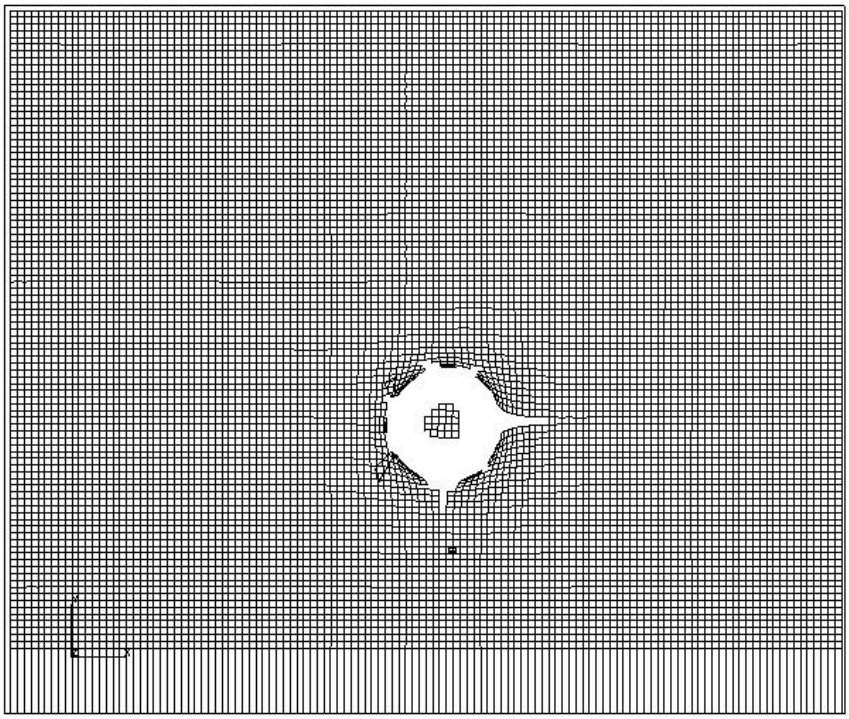

Dytran result (Nominal energy: 1500J, plate thickness 3.2 mm)